Acta Cryst. (1983). A**39**, 14–21

Electrostatic Molecular Interaction from X-ray Diffraction Data. II. Test on Theoretical Pyrazine Data

BY DIRK FEIL

Chemical Physical Laboratory, Twente University of Technology, PO Box 217, 7500 *AE Enschede, The Netherlands*

AND GRANT MOSS

Medical Foundation of Buffalo, Inc., 73 High Street, Buffalo, NY 14203, *USA*

(*Received* 8 *December* 1981; *accepted* 23 *June* 1982)

Abstract

In a previous paper [Moss & Feil (1981). *Acta Cryst.* A**37**, 414–421] a method was reported to calculate the electrostatic potential and the electrostatic interaction energy from single-crystal X-ray diffraction data. The method was applied to experimental pyrazine data; however, owing to the relatively low quality of the data, the results were inconclusive. In the present paper the results are presented of a model study in which the method has been applied to the analysis of ideal error-free diffraction data calculated from a theoretical wavefunction. The molecular quadrupole moments and the electrostatic interaction energies of two pyrazine molecules thus obtained are in very good agreement with the corresponding results derived directly from the wavefunction. Thus the proposed method may be used to determine the long-range electrostatic component of molecular interactions from highly accurate X-ray diffraction data.

Introduction

When atoms form a molecule charge is moved from one part of the molecule to another. This displacement of charge, or electron density, is an essential part of the formation of chemical bonds. Whereas the origin of this effect is well understood and its qualitative features can be predicted, its magnitude is difficult to calculate for molecules consisting of more than a few atoms.

Several properties of the molecule depend on its charge distribution. In particular, the deviation from spherical symmetry of the constituent atoms and the transfer of charge from one atom to another give rise to a potential in the region surrounding the molecule. Scrocco & Tomasi (1978) have discussed the role of this potential in the chemical reactivity of the molecule.

In a previous paper (Moss & Feil, 1981), hereafter referred to as paper I, the authors reported a method to calculate the electrostatic potential and the electrostatic interaction energy from single-crystal X-ray diffraction data. The method consists of three steps: In the first step, following Hirshfeld (1971), the electron density in the crystal, $\rho(\mathbf{r})$, is written as a linear combination of the density corresponding to free atoms, $\rho_0^{(i)}(\mathbf{r})$, and atomic deformation densities, $\Delta\rho^{(i)}(\mathbf{r})$:

$$\rho(\mathbf{r}) = \sum_i^{\text{atoms}} [\rho_0^{(i)}(\mathbf{r}) + \Delta\rho^{(i)}(\mathbf{r})].$$

The deformation densities are determined from X-ray diffraction data, along with the conventional positional and thermal parameters, in a least-squares refinement. In the second step the deformation densities are replaced by point multipole moments centered on the atoms. In the final step the electrostatic potential due to the molecule is calculated using the point multipole moments of the constituent atoms. Similarly the electrostatic interaction energy between two molecules is calculated as a series of point-multipole–point-multipole interactions. Implicit in the comparison of the results of this last step with theoretical calculations is the assumption that the electron density distribution in a crystal is the superposition of the electron density distributions of isolated molecules. Recent work by Moss & Coppens (1980) indicates that this assumption may not be entirely valid.

In paper I the method outlined above was applied to experimental X-ray diffraction data on pyrazine. The electrostatic interaction energies of two pyrazine molecules determined from the refined deformation models were in qualitative agreement with an approximate theoretical calculation based on an *ab initio* wavefunction. The poor quality of the pyrazine crystal precluded a precise determination of the deformation density with the result that several deformation models gave equally good agreement with the experiment as judged by the conventional crystallographic agreement

0567-7394/83/010014-08$01.50

factors. The corresponding electrostatic interaction energies of two pyrazine molecules, however, showed a considerable spread. Moreover, the theoretical results were outside the range of values calculated on the basis of the various deformation models. Thus no conclusive answer could be given to the question of the suitability of the proposed method to obtain electrostatic properties from X-ray diffraction data.

In the present paper we apply the method to ideal error-free diffraction data calculated from a theoretical wavefunction. We compare:

(i) the deformation model difference densities calculated at finite resolution with the difference density calculated using the theoretical structure factors;

(ii) the molecular quadrupole moments calculated from the refined deformation parameters with those calculated directly from the wavefunction; and

(iii) the electrostatic interaction energies of two pyrazine molecules calculated from a point-multipole–point-multipole series, where the point multipoles are derived from the refined deformation parameters, with the corresponding results derived directly from the wavefunction using an approximate theoretical technique.

The results of these comparisons show that the proposed method can be used to calculate the long-range electrostatic component of molecular interactions from highly accurate X-ray diffraction data.

Calculations and results

(*a*) *Structure factors*

Structure factors were calculated from the molecular wavefunction of Almlöf, Roos, Wahlgren & Johansen (1973). This wavefunction is the result of a single determinant SCF calculation using the experimental geometry determined from the spectroscopic measurements of Meritt & Innes (1960) and the following basis set: C,N [7*s*,3*p*]; contracted to [4*s*,2*p*]; H [4*s*] contracted to [2*s*], supplemented by two $p\sigma$ polarization functions. When a wavefunction is calculated, nuclear positions are used as parameters. Owing to experimental errors and the approximations in the calculations, experimental positions of the nuclei will not, in general, coincide with minimum-potential-energy positions of the nuclei. In this case, the Hellmann–Feynman theorem predicts a distribution of electron density that leads to an electrostatic force on the nuclei. This feature in the electron density appears as sharp dipole distributions centered at the nuclei. Such a sharp dipole distribution will, however, hardly be observable in the low-order data of the present calculation. The use of an experimental geometry in the theoretical calculation will therefore be of little import in the present study.

Two sets of structure factors were calculated using the experimental unit cell as given in Table 1. The structure factors belonging to the first set correspond to a static density and were assigned unit weights. Thus the information content of these structure factors is correctly represented in the least-squares refinement.

The second data set was obtained by applying an isotropic, overall temperature factor corresponding to a mean square displacement of $\langle u^2 \rangle = 0{\cdot}01$ Å^2. To this second set of structure factors variances were assigned corresponding with those derived from the experimental pyrazine data of de With, Harkema & Feil (1976):

$$\sigma^2(F_{\rm th}^2) = \frac{\sigma^2(F_{\rm obs}^2)}{F_{\rm obs}^2} F_{\rm th}^2 + \frac{1}{F_{\rm th}},$$

where $F_{\rm obs}$ and $F_{\rm th}$ are the observed and theoretical structure factors respectively and σ^2 is the variance assigned to the structure factors. The last term was added to prevent very small theoretical structure factors from having a very large weight in the least-squares refinement. Its physical significance is doubtful, but it is not expected to introduce systematic errors and it served the purpose well. Thus this second set of structure factors more closely parallels the experimental situation in which the high-order data are generally less reliable. Figs. 1(*a*) and (*b*) show the difference electron density for the two sets of structure factors.

(*b*) *Choice of deformation models*

Both sets of structure factors were analyzed using the deformation model of Hirshfeld (1971). The deformation functions centered on atom i are of the general form

$$\delta\rho_{n,k}^{(i)}(\mathbf{r}_i) = C_{n,k}^{(i)} N_n r_i^n e^{-\alpha_i r_i} \cos^n \theta_{n,k},$$

where the vector $\mathbf{r}_i$ is measured from the atomic site, $\theta_{n,k}$ is the angle between the vector $\mathbf{r}_i$ and a specified polar axis (n,k), n is the order of the function ranging from 0 to 4, $k = 1, 2, \ldots, (n+1)(n+2)/2$ and labels the polar axes of a given order, α is a parameter that governs the radial breadth of the deformation functions on each type of atom, and N_n is a normalizing factor. The parameters $\{C_{n,k}^{(i)}, \alpha_i\}$ are determined in a least-squares refinement.

The deformation functions of second and higher order are hybrid functions. For example, the six functions with $n = 2$ are linear combinations of an

Table 1. *Unit-cell information (de With, Harkema & Feil, 1976)*

$a = 9{\cdot}325$ Å	Space group No. 58, *Pmnn*
$b = 5{\cdot}850$	$Z = 2$
$c = 3{\cdot}733$	$(\sin\theta/\lambda)_{\rm max} = 1{\cdot}0$ Å^{-1}

implied monopole function, and five independent functions with the same radial dependence and an angular dependence $Y_{lm}(\theta,\varphi)$, where $l = 2$ and $m = 0$, ±1, ±2. Similarly, the third-order functions contain implied dipolar terms while the fourth-order functions contain implied monopole and quadrupolar terms.

Figs. 1(*a*) and (*b*) show negative regions about the carbon and nitrogen nuclei. It requires monopolar, or zeroth-order, deformation functions to describe these distributions. As stated above, the second- and fourth-order deformation functions contain implicit monopolar contributions; hence three terms with radial dependence $e^{-\alpha r}$, $r^2 e^{-\alpha r}$ and $r^4 e^{-\alpha r}$ are present to describe spherical distortions of the charge distributions. The differences among these various monopolar terms are most pronounced very close to the origin. The lack of resolution of experimental data makes the determination of the coefficient of the zeroth-order or explicit monopole function extremely difficult. Consequently, the explicit monopole is often omitted from the deformation model. The effect of this term was tested using deformation models with and without an explicit monopole function on C and N. In all cases an explicit monopole function was included in the hydrogen deformation model.

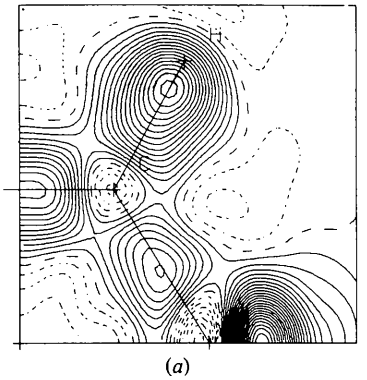

(*a*)

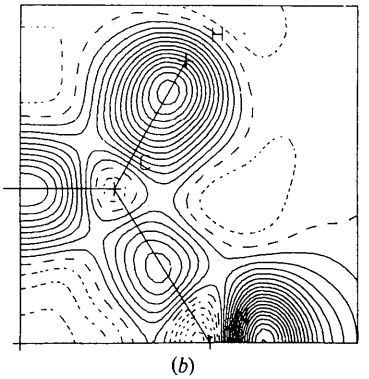

(*b*)

Fig. 1. Difference density in pyrazine calculated at limited resolution with $F_{\text{theory}} - F_{\text{spherical atom}}$ as input where F_{theory} are: (*a*) the static structure factors of data set 1, and (*b*) the thermally smeared structure factors of data set 2. The contours are at intervals of 0·05 e Å^{-3}. The contours are solid and dashed for positive and negative densities respectively.

Hirshfeld (1977) has pointed out that the potentially large number of deformation coefficients may be reduced by a consideration of local atomic symmetries. In some cases the crystallographic symmetry fixes some of the deformation coefficients. In other cases difference maps show the presence of approximate, non-crystallographic, local symmetries, which allow some parameters to be constrained. Since the wavefunction from which the test structure factors were derived was calculated for a planar molecule the electron density distribution was assumed to contain a mirror plane. The local symmetry of the C atom suggests that an additional mirror plane through the C—H bond, perpendicular to the plane of the molecule, be imposed on the C-atom deformation functions. The effect of imposing this mirror plane on the results was determined by using models with and without the mirror plane. The low electron density of the hydrogen atom and the absence of fine details in the electron distribution usually limits deformation models to at most second-order functions of the hydrogen atom. Fig. 2 shows the difference electron density distribution in a plane through the H atom perpendicular to the C—H bond. It shows approximately rotational symmetry which, to second order, is equivalent to a fourfold rotation axis along the C—H bond.

A summary of the different deformation models used is given in Table 2. The notation is in two parts. The first part denotes the presence (*M*) or absence (—) of explicit monopolar or zeroth-order deformation functions on carbon and nitrogen. The second part denotes the local symmetry imposed on the C atom as either *m*, corresponding to the molecular mirror symmetry, or *mm*, for which an additional mirror plane through the C—H bond and perpendicular to the molecular plane has been imposed.

(*c*) *Refinements*

Least-squares refinements based on F^2 were performed using the two data sets and the four defor-

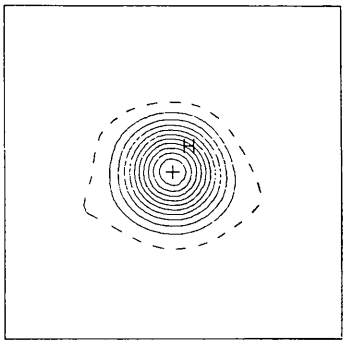

Fig. 2. Difference density through the hydrogen atom perpendicular to the carbon–hydrogen bond as calculated from data set 1. The molecular plane passes vertically through the hydrogen atom. Contours as in Fig. 1.

mation models described above. In all refinements the scale factor and the input positional and overall thermal parameters were held fixed. This limits the test to which the method is put, since it is known that these parameters correlate with the deformation parameters. Strong cases are made for using neutron parameters for positions and thermal motion, in particular for the hydrogen atoms. The discussion on the transferability of neutron parameters, however, is still in full swing and some doubt exists if these parameters will be accurate enough. The C and N spherical-atom scattering factors were taken from *International Tables for X-ray Crystallography* (1974). For hydrogen the contracted spherical-atom scattering factors of Stewart, Davidson & Simpson (1965) were used. Use of a contracted hydrogen atom in the least-squares refinement corresponds to a fixed-monopole hydrogen deformation function in addition to the parameters of the Hirshfeld deformation model. In calculating all difference and model maps an isolated spherical hydrogen atom was subtracted. To improve the convergence of the refinements, damping factors of 0·5 were applied to all parameters. The correspondence between the theoretical structure factors, F_{th}, and those based on the model, F_{mod}, is expressed by the following (dis)-agreement factors

$$R = \frac{\sum_{\mathbf{H}} |F_{th}(\mathbf{H}) - F_{mod}(\mathbf{H})|}{\sum_{\mathbf{H}} F_{th}(\mathbf{H})}$$

and

$$R_w = \left[\frac{\sum_{\mathbf{H}} w(\mathbf{H})[F_{th}^2(\mathbf{H}) - F_{mod}^2(\mathbf{H})]^2}{\sum_{\mathbf{H}} (w(\mathbf{H}) F_{th}^2(\mathbf{H}))^2} \right]^{1/2}.$$

The results of the different refinements are given in Table 3.

Table 2. *Deformation models*

	M,m	*M,mm*	*−,m*	*−,mm*
(*a*) Order of functions				
on C and N	0, 1, 2, 3, 4	0, 1, 2, 3, 4	1, 2, 3, 4	1, 2, 3, 4
on H	0, 1, 2	0, 1, 2	0, 1, 2	0, 1, 2
(*b*) Local symmetry				
on N	*mm*	*mm*	*mm*	*mm*
on C	*m*	*mm*	*m*	*mm*
on H	4*mm*	4*mm*	4*mm*	4*mm*

Table 3. *Agreement factors from multipole refinements*

Data set 1 (unit weights, no thermal smearing)

	M,m	*M,mm*	*−,m*	*−,mm*
R (%)	0·45	0·45	0·57	0·78
R_w (%)	0·34	0·52	0·63	0·78

Data set 2 (experimental weights, thermal smearing)

	M,m	*M,mm*	*−,m*	*−,mm*
R (%)	0·46	0·53	0·69	0·78
R_w (%)	0·45	0·61	0·97	1·18

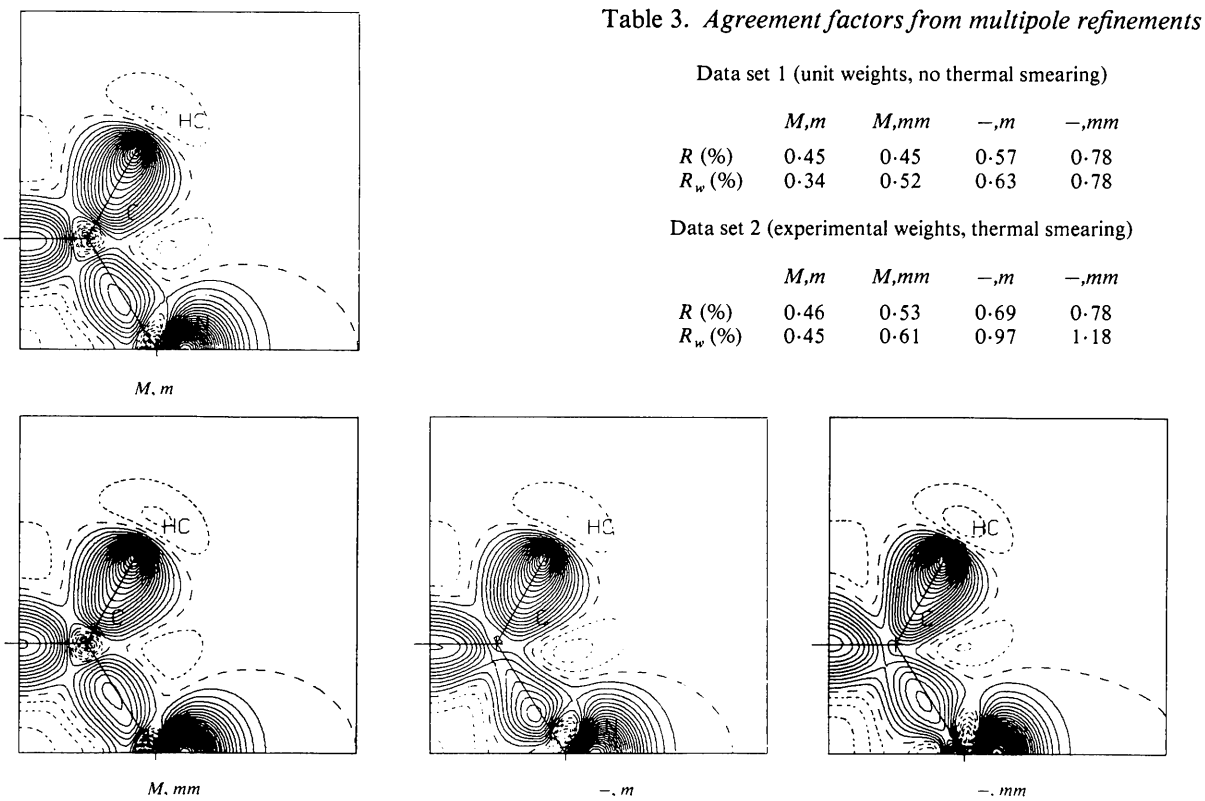

M, m *M, mm* *−, m* *−, mm*

Fig. 3. Model deformation densities $\Delta\rho_{mod}(\mathbf{r})$ at infinite resolution for the four deformation models of Table 2 from the analysis of data set 1. Contours as in Fig. 1.

(d) Electron density distribution

From the results of the refinements three kinds of electron density maps were calculated with the following input:

(1) model density distribution at infinite resolution

$$\Delta\rho_{\text{mod}}(\mathbf{r}) = \sum_{i,n,k} \delta\rho_{n,k}^{(i)}(\mathbf{r});$$

(2) model density at limited resolution

$$\Delta\rho_{\text{mod}}^{l}(\mathbf{r}) = \frac{1}{V}\sum_{\mathbf{H}}\left(F_{\text{mod}} - \sum_j f_j^{\text{atomic}}\right) e^{2\pi i\mathbf{H}.\mathbf{r}};$$

(3) residual density

$$\Delta\rho_r(\mathbf{r}) = \frac{1}{V}\sum_{\mathbf{H}} (F_{\text{th}} - F_{\text{mod}})\, e^{2\pi i\mathbf{H}.\mathbf{r}}.$$

The maps based on the different models refined using data set 1 are shown in Figs. 3, 4 and 5. In order to compare the results based on data set 2 with these maps, the static model density and the corresponding structure factors were calculated. The resulting maps showed no systematic differences from those obtained with data set 1 and are therefore not given here. As discussed above, the sharp features at the nitrogen nucleus may be due, in part, to the use of an experimental geometry in the calculation of the wavefunction.

(e) Molecular quadrupole moments

The distribution of charge in a system can be represented by its moments. The outer moments of an assembly of point charges, q_i, are defined by

$$\mu_{\alpha\beta\ldots\eta} = \sum_i q_i r_\alpha^{(i)} r_\beta^{(i)} \ldots r_\eta^{(i)},$$

where $r_\alpha = x,y,z$ for $\alpha = 1, 2, 3$.

An alternative formulation, used by Buckingham (1959), defines the outer moments of a charge distribution in terms of the Legendre polynomials. The Buckingham moments are easily derived from the outer moments. For example, the components of the quadrupole moment are simply related to the second moments through the expressions

$$\Theta_{xx} = \tfrac{1}{2}\sum_i q_i(3x_i^2 - r_i^2) = \mu_{xx} - \tfrac{1}{2}(\mu_{yy} + \mu_{zz})$$

$$\Theta_{xy} = \tfrac{3}{2}\mu_{xy}.$$

By definition the Buckingham moments are zero for an assembly of neutral spherical atoms, hence non-zero values provide a measure of the shift of electron density due to bond formation.

By symmetry the first non-vanishing moment of the pyrazine molecule is the molecular quadrupole moment. The components of the quadrupole moment can be derived from the refined deformation model density distribution $\Delta\rho_{\text{mod}}(\mathbf{r}) = \sum_{i,n,k} \delta\rho_{n,k}^{(i)}(\mathbf{r})$. The results obtained with the different deformation models are compared with the values calculated directly from the wavefunction of Almlöf, Roos, Wahlgren & Johansen (1973) in Table 4. We notice that most moments are slightly underestimated relative to the theoretical values. The largest discrepancies between the model values and those calculated directly from the wavefunction are found in model (−,*m*).

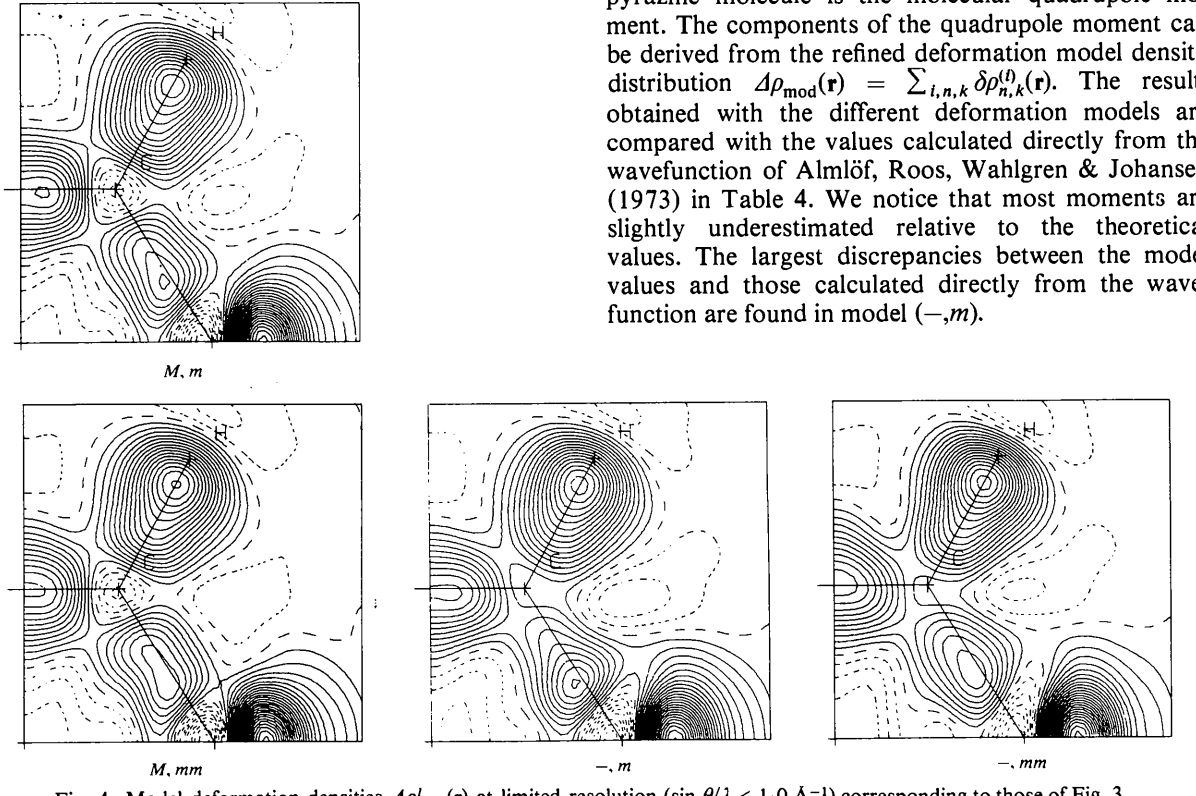

Fig. 4. Model deformation densities $\Delta\rho_{\text{mod}}^{l}(\mathbf{r})$ at limited resolution ($\sin\theta/\lambda < 1{\cdot}0$ Å^{-1}) corresponding to those of Fig. 3.

(f) Potential calculations

The electrostatic effect of the charge distribution in a molecule on neighboring charges is most directly represented by the potential in the space surrounding the molecule. To avoid complications due to penetration of the promolecule density, that is the density formed by the superposition of neutral spherical atoms, only the region outside the van der Waals radii was considered.

The electrostatic potential can be calculated by either

(i) direct solution of Poisson's equation through the expression

$$V(\mathbf{r}) = \frac{-|e|}{4\pi\varepsilon_0} \int \frac{\Delta\rho_{\text{mod}}(\mathbf{r})}{\mathbf{r}} \, \mathrm{d}\mathbf{r}$$

or

(ii) by expanding this expression as a series involving point multipole moments centered at the nuclear sites (Buckingham, 1959), where these point multipoles are derived from the spatially extended atom-centered deformation functions.

Calculations showed no difference between the results of the two methods at the distances of interest here. The potential, corresponding with model (*M,m*), expressed as the potential energy of a proton in the field of the molecule, is shown in Fig. 6. The difference from the results obtained with other deformation models are shown in Fig. 7. Since the results obtained from the analysis of the two data sets are very similar only those for data set 1 are presented here.

(g) Electrostatic energy

As in the case of the potential, the electrostatic interaction energy can be expressed as a series involving the point multipoles (Buckingham, 1959). In this expression, which is valid for large molecular

Table 4. *Molecular quadrupole moments (atomic units)*

The x axis is along the N–N vector and the molecule lies in the xy plane. Also note that by definition $\Theta_{zz} = -(\Theta_{xx} + \Theta_{yy})$.

	M,m	*M,mm*	*−,m*	*−,mm*	Theoretical*
Θ_{xx}	−8·35	−8·68	−7·36	−8·43	−8·91
Θ_{yy}	10·15	10·01	9·01	9·85	10·38
Θ_{zz}	−1·80	−1·32	−1·65	−1·41	−1·47

* Calculated from the wavefunction of Almlöf, Roos, Wahlgren & Johansen (1973).

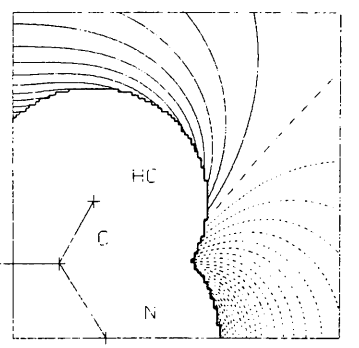

Fig. 6. Deformation electrostatic potential calculated with model (*M,m*) from the analysis of data set 1. The contours are at intervals of 2 kcal mol^{-1} (8·37 kJ mol^{-1}). The contours are solid and dashed for positive and negative values respectively. The long-dash line is the zero contour. The solid border is formed by the intersection of 1·7 Å spheres centered at each atomic site and corresponds approximately to the van der Waals surface of the molecule.

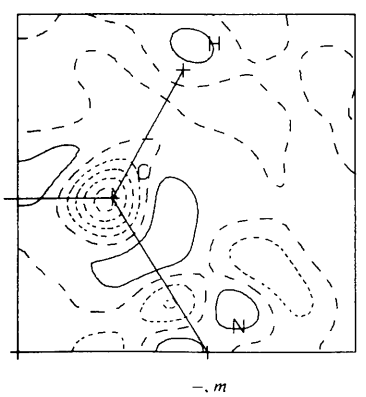

−, *m*

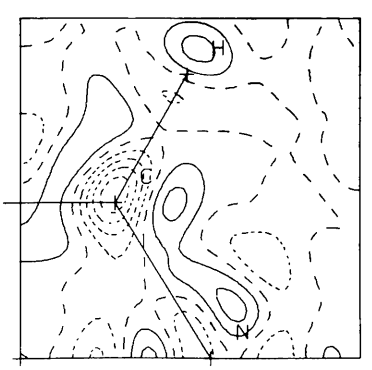

−, *mm*

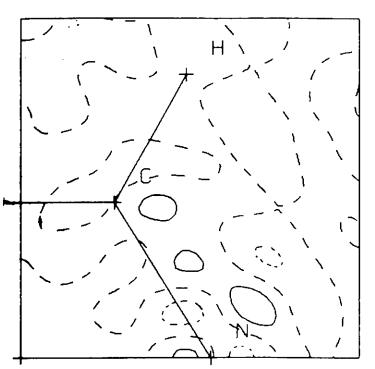

M, m

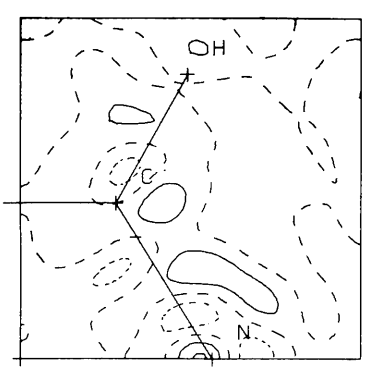

M, mm

Fig. 5. Residual densities $\Delta\rho_r(\mathbf{r})$ corresponding to the model densities of Fig. 4. Contours as in Fig. 1.

separations, point charges interact with the electrostatic potential; point dipoles with the electric field; point quadrupoles with the electric field gradient; and so on. The various formulae needed are given in paper I.

The results based on data set 1 are given in Fig. 8 and those based on data set 2 in Fig. 9. For comparison the theoretical calculation of Mulder & Huiszoon (1977) from the wavefunction of Almlöf *et al.* (1973) is also included. As the curve for models (*M*,*m*), (*M*,*mm*) and (−,*mm*) essentially superpose, only those for models (*M*,*m*) and (−,*m*) are shown.

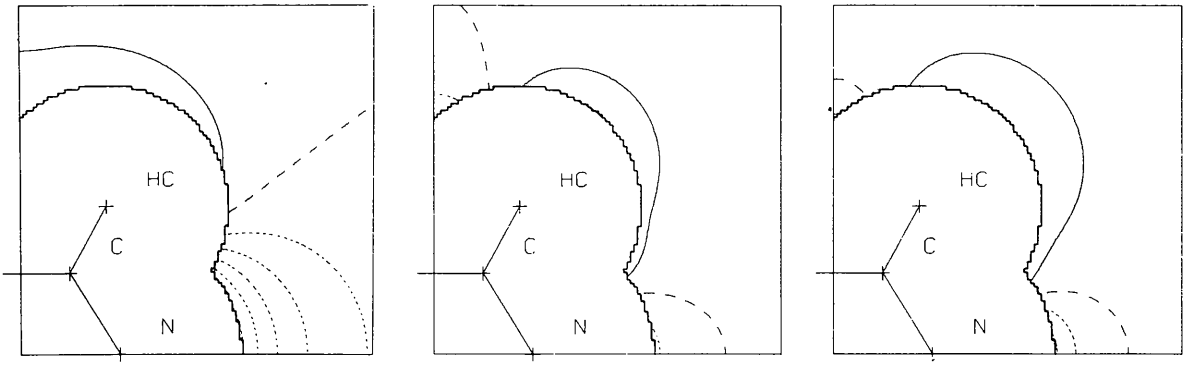

(*a*) (*b*) (*c*)

Fig. 7. Differences between the electrostatic potential of model (*M*,*m*) and (*a*) model (−,*m*), (*b*) model (*M*,*mm*) and (*c*) model (−,*mm*). The contours are at 1·0 kcal mol^{-1} (4·19 kJ mol^{-1}) intervals.

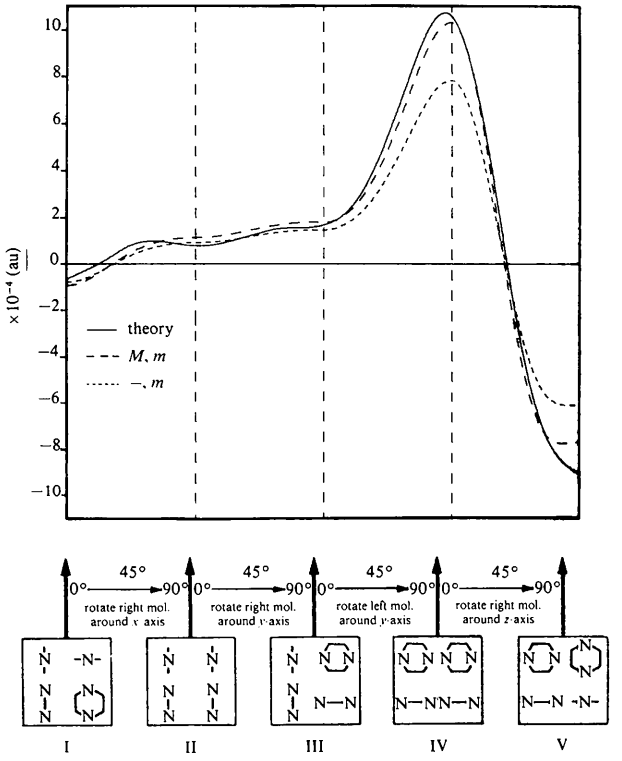

Fig. 8. Electrostatic interaction energy of two pyrazine molecules at a fixed center-of-mass separation of 15 a.u. The relative orientation of the molecules is indicated at the bottom of the figure. The solid curve is the theoretical result of Mulder & Huiszoon (1977). The dashed curves are calculated from the results of the multipole refinements of data set 1.

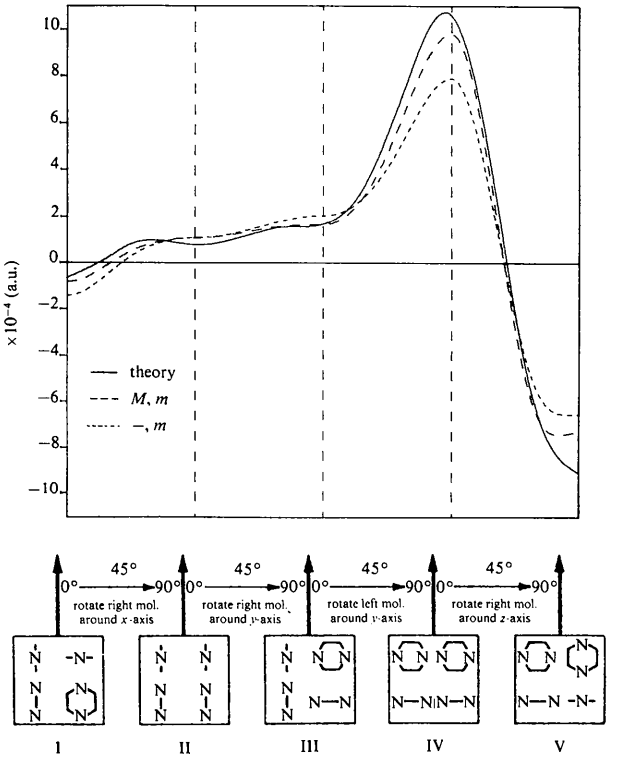

Fig. 9. Electrostatic interaction energy of two pyrazine molecules at a fixed center-of-mass separation of 15 a.u. The relative orientation of the molecules is indicated at the bottom of the figure. The solid curve is the theoretical result of Mulder & Huiszoon (1977). The dashed curves are calculated from the results of the multipole refinements of data set 2.

Discussion and conclusions

As is seen from the R factors, none of the deformation models has enough flexibility to fit the electron density distribution perfectly. As can be expected, the most flexible model, (M,m), gives the best fit. Data set 2, in which the high-order data are smaller in magnitude and, consequently, contribute less to the R factor, shows only slightly inferior agreement, reflecting the fact that the effects of the deformation density are most felt in the low-order region.

The residual maps of the models including an explicit zeroth-order function, (M,m) and (M,mm), show little significant structure. Understandably, the mirror plane along the C–H bond imposed on the carbon deformation functions makes determination of unsymmetric features difficult, particularly in the C–H region where the hydrogen atom also has imposed mirror symmetry. Both $(-,m)$ and $(-,mm)$ residual maps show the need of an explicit monopole or zeroth-order function in the model.

The similarity between the model maps at limited and at infinite resolution shows that the significant features of the models are contained in the low-order data. It is the electron density distribution shown in the maps at infinite resolution and summarized in point multipoles on which the molecular quadrupole moment, potential and interaction energy calculations are based.

The generally good agreement between the model quadrupole moments and those calculated directly from the wavefunction is an indication of the high quality of the models. The slight underestimate relative to the theoretical values is consistent with the results of Moss & Coppens (1982); however, there appears to be no rational explanation for the larger underestimation obtained with model $(-,m)$ than with the other models.

The potential maps of Fig. 7 show only slight differences. Stewart (1979) has shown that the potential can be calculated by Fourier summation using $F(\mathbf{H})/\mathbf{H}^2$ as coefficients. Thus the potential is determined to a large extent by the low-order data. Consequently, the much discussed sharply featured monopole functions have only minor influence on the potential.

The interaction energy between two molecules depends both on the potential in the region beyond the molecular boundaries and on the charge distribution in the molecule. We notice that model $(-,m)$ with its deficient quadrupole moment deviates from the highly similar results obtained by the other models.

The differences between the results of Mulder & Huiszoon (1977) and the present results are small over most of the different orientations. The origin of these differences may be due both to the slight underestimation of the multipole moments and to differences in the respective methods of calculation. The calculation of Mulder & Huiszoon (1977) was based on the interaction between molecular point multipoles for which the sum of the orders of the multipoles on the two interacting molecules did not exceed seven. In the present work the calculation is based on the interaction between atomic-centered multipoles, thus the series expansion of the electrostatic interaction energy employed here is carried to a larger number of terms than that of Mulder & Huiszoon (1977).

The results of the present study show that the distortion of the electron density distribution, which is the inevitable consequence of its representation in terms of a finite atom-centered expansion, is of minor consequence. The compact explicit monopole functions, indicated by the residual density maps, appear to have little effect on the long-range electrostatic potential or interaction energy calculations. It is these sharp atom-centered features which are extremely difficult to determine from experimental data because, firstly, errors in the electron density distribution due to errors in the experimental determination of the structure factors accumulate in the nuclear region and, secondly, due to the limited resolution of the experiment, only a part of the electron density in the nuclear region is represented in the diffraction data.

We therefore conclude that the present method opens the possibility of determining interaction parameters from highly accurate X-ray diffraction data.

This work was mostly done while GM was a Research Fellow at Twente University of Technology. It was produced in its final form while DF was a guest of the Medical Foundation of Buffalo, to whom he is grateful. This work was supported, in part, by NSF grant CHE79-11282 and DHEW grant GM-26195. The authors wish to thank Dr R. H. Blessing for his critical reading of the manuscript, Ms Melda Tugac and Ms Gloria Del Bel for the excellent diagrams and Ms Brenda Giacchi for her perseverence in typing the manuscript.

References

ALMLÖF, I., ROOS, B., WAHLGREN, Y. & JOHANSEN, H. (1973). *J. Electron Spectrosc. Relat. Phenom.* **2**, 51–74.

BUCKINGHAM, A. D. (1959). *Q. Rev. Chem. Soc.* **13**, 183–214.

HIRSHFELD, F. L. (1971). *Acta Cryst.* B**27**, 769–781.

International Tables for X-ray Crystallography (1974). Vol. IV. Birmingham: Kynoch Press.

MERRITT, J. A. & INNES, K. K. (1960). *Spectrochim. Acta*, **16**, 945–953.

MOSS, G. & COPPENS, P. (1980). *Chem. Phys. Lett.* **75**, 298–302.

MOSS, G. & COPPENS, P. (1982). In preparation.

MOSS, G. & FEIL, D. (1981). *Acta Cryst.* A**37**, 414–421.

MULDER, F. & HUISZOON, C. (1977). *Mol. Phys.* **34**, 1215–1235.

SCROCCO, E. & TOMASI, J. (1978). *Adv. Quantum Chem.* **11**, 115–193.

STEWART, R. F. (1979). *Chem. Phys. Lett.* **65**, 1215–1235.

STEWART, R. F., DAVIDSON, E. F. & SIMPSON, W. T. (1965). *J. Chem. Phys.* **42**, 3175–3187.

WITH, G. DE, HARKEMA, S. & FEIL, D. (1976). *Acta Cryst.* B**32**, 3178–3184.